RSC Advances

Solvatochromic studies of pull-push molecule containing dimethylaniline and aromatic hydrocarbon linked by acetylene unit

Journal:	*RSC Advances*
Manuscript ID:	RA-ART-07-2014-006999.R2
Article Type:	Paper
Date Submitted by the Author:	15-Sep-2014
Complete List of Authors:	Wiczk, Wieslaw; University of Gdansk, Chemistry Wierzbicka, Malgorzata; University of Gdansk, Chemistry Bylinska, Irena; University of Gdansk, Chemistry Czaplewski, Cezary; University of Gdansk, Chemistry

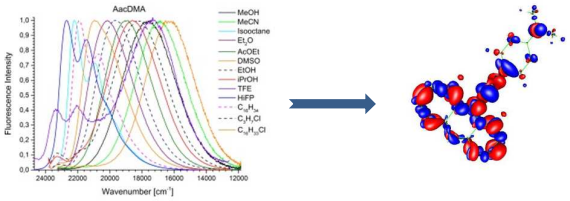
AacDMA
Fluorescence Intensity
Wavenumber [cm⁻¹]
MeOH
MeCN
Isooctane
Et2O
AcOEt
DMSO
EtOH
iPrOH
TFE
HFP

Solvatochromic studies of pull-push molecule containing dimethylaniline and aromatic hydrocarbon linked by acetylene unit

Irena Bylińska, Małgorzata Wierzbicka, Cezary Czaplewski, Wiesław Wiczk*

Faculty of Chemistry, University of Gdańsk

80-308 Gdańsk, Wita Stwosza 63, Poland

* corresponding author

e-mail: wieslaw.wiczk@ug.edu.pl

Abstract

Pull-push molecules containing dimethylaniline and aromatic hydrocarbon linked by acetylene unit were studied using spectroscopic methods and DFT theoretical calculations. Spectral and photophysical properties of N,N-dimethyl-4-(naphtalen-1-ylethynyl)aniline, N,N-dimethyl-4-(naphtalen-2-ylethynyl)aniline, 4-(athracen-9-ylethynyl)-N,N-dimethylaniline were studied in 26 solvents (non-polar, polar aprotic and protic). The influence of solvents properties on spectral and photophysical properties of compounds studied was analyzed using empirical Riechardt`s solvent polarity index as well as Catalán and Kamlet-Tatf multi-parameter solvent scales. The change of the dipole moment in the excited state was estimated basing on Bilot-Kawski theory. Using the solvatochromic method, the change of hydrogen bond energy in the excited state was calculated. Theoretical calculations confirm the conclusions arising from experimental studies.

1. Introduction

So-called pull-push chromophores containing electron donor and acceptor connected by π-electron bridge (D-π-A) are of substantial interest for optoelectronic devices[1]. They were used as components of light-emitting diodes[2-4], solar cells[5-8], or electrogenerated chemiluminescence[9-14]. Also, this class of compounds shows large nonlinear optical response (NLO) which allows to use it for second-order NLO applications[1,15,16].

Pull-push chromophores are polar fluorescent molecules which offer the opportunity to use them as a fluorescent probes (solvation probes) in the studies of solute-solvent interactions[17]. Such compounds are presented in this paper N,N-dimethyl-4-(naphtalen-1-ylethynyl)aniline (1NacDMA), N,N-dimethyl-4-(naphtalen-2-ylethynyl)aniline (2NacDMA), 4-(athracen-9-ylethynyl)-N,N-dimethylaniline (AacDMA) (Fig. 1) which have been already studied as materials for organic light emitting diode, with the main emphasis on electrochemiluminescence[9]. However, solvatochromic studies of these compounds have been limited to a small number of solvents, therefore, a more detailed study is still necessary in order to understand the phenomenon of solute-solvent interactions and photophysical characteristic of a donor-acceptor molecule with a triple bond as a bridge between the donor and the acceptor. Our research covers a wide group of solvents (26) including nonpolar and polar as well as protic and aprotic ones (see Table 1 ESI for the list of solvents used, their abbreviations and properties). The impact of the microenvironment on photophysical properties was determined basing on the single empirical and multiple parametric solvent scales. The change of the hydrogen bond energy of the molecule in the Franck-Condon and relaxed S_1 excited state is analyzed. Moreover, the dipole

moments of the compounds studied in the excited state are determined. It is essential to better evaluate the macroscopic hyperpolarizability in view of applications.

2. Theoretical background

2.1 Solvent polarity scales

A general model which describes the properties of solvent and salvation does not exists. As a result, several empirical solvent polarity scales have been proposed to characterize and rank empirically the polarity of the solvent.

One of the most popular solvent polarity scale is the one parameter solvent polarity scale $E_T(30)$ or the normalized E_N^T parameter defined according to equation:

$$E_T^N = \frac{E_T(solvent) - E_T(TMS)}{E_T(water) - E_T(TMS)} \quad (1)$$

where, TMS denoted tetramethylsilane, introduced by Reichardt et al.[18,19].

The $E_T(30)$ values, empirically derived from solvatochromic measurements, are simply defined as the molar transition energies (in $kcalmol^{-1}$) of the standard pyridinium N-phenolate betaine dye, measured in solvents of different polarity at room temperature (25 ºC) and normal pressure (1 bar), according to eq. (2):

$$E_T(30)(kcal/mol) = 28591/\lambda_{max}(nm) \quad (2)$$

where λ_{max} is the wavelength of the maximum of the long-wavelength intramolecular CT absorption band of the betaine.

The $E_T(30)$ or E_N^T parameter is widely used to measure empirically the polarity of many systems. It is also frequently used as a parameter of linear solvation energy relationships for the correlation analysis of solvent effect on chemical and physical

properties[18-22]. For non-hydrogen bond donor solvents, $E_T(30)$ or E_N^T parameter describes almost exclusively the electrostatic forces between solute and solvent[23]. Apart from the dependence of different spectral and photophysical properties on E_N^T parameter, the correlation of the Stokes shift with this parameter can be applied to calculate the dipole moment change between the excited and ground state based on the equation proposed by Ravi et al.[24,25] :

$$\Delta\tilde{\nu} = \tilde{\nu}_a - \tilde{\nu}_f = 11307.6\left[\left(\frac{\Delta\mu}{\Delta\mu_B}\right)^2\left(\frac{a_B}{a}\right)^3\right]E_T^N + const \qquad (3)$$

where $\Delta\mu_B$ and a_B are the dipole moment change and Onsager's radius, respectively, for a pyridinium N-phenolatebetaine dye used to determine the E_N^T values ($\Delta\mu_B$ =9 D and a_B=6.2 Å), whereas $\Delta\mu$ and *a* are the corresponding quantities for the molecule under study. The advantage of this equation is to minimize the problem associated with the Onsager`s radius estimation since a ratio of two Onsager`s radii is involved in the equation.

To study solute-solvent interactions also multiparameter solvent polarity scales are widely used. The multiple linear regression approach, introduced by Kamlet-Taft and co-workers[26], has been used to correlate UV–Vis absorption and emission energies with an index of the solvent dipolarity/polarizability, which is a measure of the solvent's ability to stabilize a charge or dipole through nonspecific dielectric interactions (π^*), and indices of the solvent's hydrogen-bond donor strength (α), and hydrogen-bond acceptor strength (β), according to eq. (4):

$$y = y_0 + a_{\pi^*}\cdot\pi^* + b_\alpha\cdot\alpha + c_\beta\cdot\beta \qquad (4)$$

Another solvent polarity scale introduced by Catalán[27], is a four-parameters solvent polarity empirical scale according to the equation:

$$y = y_0 + a_{SP} \cdot SP + b_{SdP} \cdot SdP + c_{SA} \cdot SA + d_{SB} \cdot SB \quad (5)$$

where: y denoted a solvent-dependent physicochemical property in a given solvent and y_0 the statistical quantity corresponding to the value of property in the gas phase; SP, SdP, SA, and SB represent independent solvent parameters accounting for various types of solute-solvent interactions (SP denotes solvent polarizability, SdP – solvent dipolarity, SA - solvent's hydrogen-bond donor strength and SB - hydrogen-bond acceptor strength); a_{SP}, b_{SdP}, c_{SA}, and d_{SB} are adjustable coefficients that reflect the sensitivity of the physical quantity y in a given solvent to the various solvent parameters.

2.2 Specific solute-solvent interactions

In a series of publications Maciejewski and co-workers[28-31] have presented a method to extract the contribution of specific interactions between solute and hydrogen-bonding solvent based on solvatochromic data.

The first step in this method requires determination of the contribution of non-specific interactions based only on solvatochromic shift of absorption and emission spectra of compound studied. The solvents used for the estimation of non-specific interactions are 1-chloro-n-alkanes which interact only non-specifically because they do not have π-electron, and charge-transfer character, and do not form hydrogen bond[28]. The straight-line obtained from solvatochromic studies of solute in 1-chloro-n-alkanes describes the effect of non-specific interactions on the values of ν_{abs}^{max} and ν_{fluo}^{max} not only in these solvents but also for all solvents studied. The distance

between the experimental ν_{abs}^{max} or ν_{fluo}^{max} values and the straight line describes the changes in the energy of hydrogen bond in Franck-Condon excited state (from ν_{abs}^{max} dependence) or relaxed excited state (from ν_{fluo}^{max} dependence) in a given solvent according to equation (6)[28]:

$$\Delta\nu_{shift}^{abs}(H-bond) = \nu_{\max}^{abs}(f(\varepsilon,n^2)) - \nu_{\max}^{abs}(\exp)$$
$$\Delta\nu_{shift}^{fluo}(H-bond) = \nu_{\max}^{fluo}(f(\varepsilon,n^2)) - \nu_{\max}^{fluo}(\exp) \quad (6)$$

where: ν_{abs}^{max}(exp) and $\nu_{\mathrm{fluo}}^{\max}$(exp) are experimental positions of the maxima of absorption and fluorescence spectra of the solute in the solvent with ability to form hydrogen bond, whereas $\nu_{\mathrm{abs}}^{\max}(f(\varepsilon,n^2))$ and $\nu_{fluo}^{max}(f(\varepsilon,n^2))$ are the values of predicted maxima of absorption and fluorescence spectra of the solute for the value of orientation polarizability function $f(\varepsilon,n^2)$ corresponding to this solvent. Thus, it is a convenient method to quantify the relative contributions from these two effects.

2.3 Determination of excited state dipole moment of molecule by solvatochromic method

In case of different electron densities in the electronic ground and excited state of a light-absorbing molecule, its dipole moment varies in these two states. Thus, a change of the solvent affects the ground and excited state differently. For non-polarizable solute, a linear dependence of absorption and emission frequency on the solvent polarity is predicted. Taking into consideration the linear and quadratic Stark`s effect for spherical molecules with a radius *a*, and isotropic polarizability α of a molecule, following equations, obtained by Bilot-Kawski[32-34], allow to compute dipole moment in the excited state:

$$\tilde{\upsilon}_a - \tilde{\upsilon}_f = m_1 f_{BK}(\varepsilon_r, n) + const \quad (7)$$

$$\tilde{\upsilon}_a + \tilde{\upsilon}_f = -m_2[f_{BK}(\varepsilon_r, n) + 2g(n)] + const \quad (8)$$

With approximation that the polarizability α of the solute is such that: $2\alpha/4\pi\varepsilon_0 a^3$=1, the solvent polarizability functions $f_{BK}(\varepsilon_r,n)$ and $g(n)$ are given by eqs (9) and (10):

$$f_{BK}(\varepsilon_r, n) = \frac{2n^2+1}{n^2+2}\left(\frac{\varepsilon_r - 1}{\varepsilon_r + 2} - \frac{n^2-1}{2n^2+1}\right) \quad (9)$$

$$g(n) = \frac{3(n^4-1)}{2(n^2+2)^2} \quad (10)$$

Using a slope obtained from eqs (7) and (8) and knowing the ground-state dipole moment μ_g, the excited-state dipole moment μ_e, can be calculated using eqs (11) and (12).

$$m_1 = \frac{(\vec{\mu}_e - \vec{\mu}_g)^2}{2\pi\varepsilon_0 hca^3} = \frac{(\mu_e^{\,2} + \mu_g^{\,2} - 2\mu_e\mu_g\cos\Psi)}{2\pi\varepsilon_0 hca^3} \quad (11)$$

$$m_2 = \frac{(\mu_e^{\,2} - \mu_g^{\,2})}{2\pi\varepsilon_0 hca^3} \quad (12)$$

In these equations μ_e and μ_g are the dipole moments in the excited and ground state, respectively, ***a*** is Onsager`s interaction radius of the solute, $h$ is Planck`s constant, c is the velocity of light in vacuum, n - refractive index, ε_r - relative dielectric constant and ε_0 is the permittivity of vacuum, thus $2\pi\varepsilon_0 hc$=1.105110440*10^{-35} C^2.

Generally, the dipole moments μ_e and μ_g are not parallel to each other but make an angle Ψ. The use of eqs (11) and (12) leads to:

$$\mu_e = \sqrt{(\mu_g^{\,2} + \frac{1}{2}m_2 hca^3)} \quad (13)$$

$$\cos\Psi = \frac{1}{2\mu_e\mu_g}\left[(\mu_g{}^2 + \mu_e{}^2) - \frac{m_1}{m_2}(\mu_g{}^2 - \mu_e{}^2)\right] \qquad (14).$$

3. Materials and methods

3.1 Synthesis

General procedure for the synthesis of 1NacDMA, 2NacDMA and AacDMA

All compounds were prepared by Sonogashira reaction according to the method described in the literature based on the coupling of 4-ethynyl-N,N-dimethylaniline with bromoarene[35-37]. Stirred solution of appropriate bromoarene (1 eq) and triethylamine (5 eq) in DMF was degassed by purging with argon. Then the catalysts, tetrakis(triphenylphosphine)palladium(0) (0.05 eq) and copper iodide (0.1 eq), were added. After re-deoxygenation of the solution, 4-ethynyl-N,N-dimethylamine (2 eq) was added. The reaction mixture was stirred at about 55°C for four days. Progress of the reaction was monitored by TLC (Kieselgel 60 F_{254}, Merck). After the reaction was completed, the crude product was filtered, diluted with toluene and washed with water and brine, and dried over anhydrous magnesium sulfate. The solvent was removed under reduced pressure. The pure products were isolated by column chromatography (Kieselgel 60, 0.040-0.063 mm, Merck, petroleum ether/ethyl acetate; 15:1 as an eluent).

All synthesized compounds were characterized by ^{1}H NMR, ^{13}C NMR spectroscopy, LCMS-IT-TOF mass spectra, FTIR and FT Raman spectroscopy. ^{1}H NMR, ^{13}C NMR spectra and melting temperature were in agreement with data published by Ho et al.[9]

3.2 Spectroscopic measurements

The UV/Vis absorption spectra of 1NacDMA, 2NacDMA and AacDMA in all 26 solvents studied were measured using a Perkin-Elmer Lambda 40P spectrophotometer, whereas emission spectra were measured using a FluoroMax-4 Horriba-Yobin Yvon spectrofluorimeter. Solvents of the highest available quality (spectroscopic or HPLC grade) were used. Fluorescence quantum yields (*QY*) were calculated with quinine sulphate in 0.5 M H_2SO_4 (*QY*= 0.53 ± 0.02) for 1NacDMA and 2NacDMA and fluorescein in 0.1 M NaOH (QY=0.95±0.03) for AacDMA as reference and were corrected for different refractive indices of solvents[38]. In all fluorimetric measurements, the optical density of the solution does not exceed 0.1. The fluorescence lifetimes were measured using a time-correlated single-photon counting apparatus CD-900 (Edinburgh Analytical Instruments) using a NanoLed (λ=339 nm or λ=375 nm) from IBH or using FT300 (PicoQuant) with subnanosecond pulsed diode PLS 340 or picosecond diode laser LDH-P-C-420 as the excitation source. The half-width of the response function of the apparatus, measured using a Ludox solution as a scatter, was about 1.0 ns for diode and about 150 ps for a laser. The emission wavelengths were isolated using a monochromator. Fluorescence decay data were fitted by the iterative convolution to the sum of exponents according to eq. (15): $I(t) = \sum_i \alpha_i \exp(-t/\tau_i)$ (15)

where α_i is the pre-exponential factor obtained from the fluorescence intensity decay analysis and τ_i the decay time of the i-th component, using a software supported by the manufacturer. The adequacy of the exponential decay fitting was judged by visual inspection of the plots of weighted residuals as well as by the statistical parameter χ^2_R and shape of the autocorrelation function of the weighted residuals and serial variance ratio (SVR).

Linear and multi-parametric correlations were performed using Origin v. 9.0 software.

3.3 Theoretical calculations

All calculations were performed using density functional theory (DFT) within Turbomole v. 6.4 suite programs on a PC cluster. The structures of all compounds were prepared and initially optimized using TmoleX program. Energy-minimum structures were searched for the ground states (S_0) using a B3-LYP hybrid functional with def2-TZVP basis set of triple-ζ quality. This procedure was considered satisfactory if the energy difference between optimized cycles was $<1*10^{-6}$ Hartree for ground state structure optimization and $<1*10^{-7}$ Hartree for excited state structure optimization. In both states a gradient of $<1*10^{-3}$ au was achieved. The low-lying excited states were treated within the adiabatic approximation of time-dependent density functional theory (TDDFT) using B3-LYP functional. The geometry optimization of the excited state was performed using grid parameter equal to 4. The convergence of all systems studied was checked by harmonic vibrational analysis. No imaginary frequencies were observed.

In addition, TD DFT calculation was carried out at the geometry of the ground state for the first 15 transitions in order to simulate the absorption spectrum in the Franck–Condon region. In order to take into account the solvent effects on the geometry and spectral shifts of UV–Vis spectra, all calculations were carried out using COSMO model implemented in TURBOMOLE program.

4 Results and discussion

4.1 Absorption spectroscopy

Absorption spectra of compounds studied in selected solvents are presented in Figs 2-4. For naphthalene derivatives (1NacDMA and 2NacDMA), first absorption band is located around 27780 cm^{-1} whereas for AacDMA at about 23260 cm^{-1} with a weakly marked vibronic structure. The increase of solvent polarity causes the bathochromic shift of the spectrum for about 750 cm^{-1} for naphthalene derivatives and 550 cm^{-1} for AacDMA. Absorption spectra measured in the highly proton-donor solvent like HFiP or TFE are shifted toward the higher wavenumber and have pronounced vibronic structure. First absorption band in TFE is at 30770 cm^{-1}, 29500 cm^{-1} and 23930 cm^{-1} for 2NacDMA, 1NacDMA and AacDMA, respectively. A shoulder on the lower wavenumber part of the spectra is present (Figs 2-4). In HFiP the absorption spectra are hipsochromically shifted comparing to these in TFE. A blue-shift of the absorption spectra in per-fluorinated alcohols is caused by the formation of hydrogen bond with electron lone pair of nitrogen atom of amino group and thereby reducing its coupling with aromatic system. Therefore, it seems that a shoulder observed in the absorption spectra in TFE is caused by the presence of molecules which do not form a strong hydrogen bond with a solvent.

4.2 Steady-state fluorescence spectroscopy

Fluorescence spectra in selected solvents are presented in Figs 5-7. In non-polar solvents, substantial asymmetry between absorption and emission spectra is observed. Such phenomenon occurs not only for the arylethynyl derivatives of N,N-dimethylaniline (DMA)[8,39], but also for phenylene ethynylene oligomers[40-44] and have been explained in terms of torsional disorder and quadratic coupling between the ground and the first excited state[45] or the exciton model developed by Liu et al.[46,47].

The increase of solvent polarity causes bathochromic shift of emission spectra and disappearance of their vibronic structure. For both naphthalene derivatives spectra shift from about 27400 cm^{-1} for *iso*-octane to 20000 cm^{-1} in DMSO, whereas for AacDMA from 22200 cm^{-1} to 16300 cm^{-1}. Such large solvatochromic effect indicates substantial increase of the excited state dipole moment. Emission spectra of studied compounds measured in per-fluorinated alcohols are different from those measured in other protic solvents. In TFE, a broad unstructured emission band is observed with a maximum similar to that in methanol, however, half-width of the emission band of naphthalene derivatives is larger than in alcohols studied (Table 2 ESI). This is probably a result of emissions of different hydrogen-bonded individuals present in the solution. For AacDMA in TFE, double emission band with maxima at about 17250 cm^{-1} and 23250 cm^{-1} is observed. Lower-wavenumber band is similar to that in methanol and its half-width (3750 cm^{-1}) is similar to other alcohols studied. The structured higher-wavenumber band almost overlaps with the emission spectrum of protonated form of AacDMA (Fig.1 ESI). Among solvents studied, HFiP is the one with the highest proton donor ability (Table 1 ESI). In this solvent naphthalene derivatives have a broad blue-shifted emission spectra with maximum at 26900 cm^{-1} and 26700 cm^{-1} for 2NacDMA and 1NacDMA, respectively, while AacDMA shows a strong blue fluorescence with maximum at 22700 cm^{-1} with well-formed vibronic structure (Fig. 2 ESI).

Fluorescence quantum yields of compounds studied are high in all polar aprotic and non-polar solvents. In protic solvents fluorescence quantum yields are low for naphthalene derivatives and depend on alcohol polarity (Tables 1-3), while for AacDMA are high, except in TFE.

4.3 Time resolved fluorescence

The fluorescence intensity decay times are summarized in Tables 1-3 for 1NacDMA, 2NacDMA and AacDMA, respectively. Fluorescence lifetimes of naphthalene derivatives are in the range from about 1 to 1.5 ns, except for most polar solvents like acetonitrile, DMF (about 3 ns) or DMSO (about 4 ns) (Tables 1 and 2), whereas for AacDMA are in the range from 2.5 to 4.5 ns (Table 3). Moreover, fluorescence intensity decay of AacDMA in HFiP is bi-exponentials with lifetime equal to 2.58 ns and 0.50 ns with the second pre-exponential factor negative (A_1=14439, A_2=-4263) indicating on the prototropic equilibrium in the excited state. Radiative and non-radiative rate constants calculated according to equations: $k_f = \Phi / \tau$ and $k_{nr} = (1-\Phi)/\tau$ are presented also in Tables 1-3. Radiative rate constant values for both naphthalene derivatives are in the range from $2*10^8$ s^{-1} to $9*10^8$ s^{-1} with the largest values in saturated hydrocarbon solvents, while for AacDMA these values are less diversified (from $8*10^7$ s^{-1} to $2.6*10^8$ s^{-1}). Values of non-radiative rate constant, k_{nr}, varies in large range (Tables 1-3). The highest values are for protic solvents, whereas the lowest for saturated hydrocarbon solvents. In polar aprotic solvents, they are close to each other.

5. Solvatochromic analysis

5.1 Correlation with Reichardt's E_N^T solvent polarity index

To study solute-solvent interactions the maxima of absorption and emission spectra, Stokes shift, fluorescence quantum yields and lifetimes, radiative and non-radiative rate constants as well as the transition dipole moments have been correlated with the microscopic solvent polarity index E_N^T. The plot of dependence of wavenumber of absorption maximum *versus* E_N^T reveals rather weak correlation for all compounds studied (Table 3 ESI, Figs 3-5 ESI). Even separate analysis of the data

for the protic and aprotic solvents does not improve the quality of fit. Better correlations with Reichardt`s solvent polarity index were obtained for the position of emission maximum. However, the experimental points for protic solvents strongly deviate from the remaining solvents (Table 3 ESI, Figs 6-8 ESI), especially for TFE and HFiP. Therefore, the data for the protic and aprotic solvents were analyzed separately. The correlation coefficient is high for both aprotic ($r^2 \approx 0.95$) and protic solvents ($r^2 \geq 0.96$) (for AacDMA the long-wavelength emission band in TFE was taken into account) (Table 3 ESI). Also, the Stokes shift well correlates with the E_N^T for both aprotic solvents ($r^2 > 0.94$, N=16) and protic solvents ($r^2 > 0.94$, N=4, excluding HFiP) (Table 3 ESI, Figs 9-11) for all compounds studied. The dependence of fluorescence quantum yield on E_N^T does not give a good correlation for all compounds studied (Figs 12-14, Table 3 ESI), except for AacDMA in protic solvents ($r^2 = 0.99$, excluding HFiP).

For naphthalene derivatives, a moderately good linear correlation of fluorescence lifetime with E_N^T is observed ($r^2 \approx 0.8$, Table 3 ESI, Figs 15-17 ESI). For AacDMA much worse correlation for aprotic solvents was obtained ($r^2 \approx 0.5$) except for protic solvents ($r^2 \approx 1.0$, without HFiP).

Both fluorescence quantum yield and fluorescence lifetime are complex function of radiative (k_f) and non-radiative (k_{nr}) rate constants. Therefore, an analysis of these rate constants as a linear function of E_N^T was performed to receive information which of them and how depends on the solvent parameters. It was found that the radiative rate constant reasonably well correlated with E_N^T ($r^2 > 0.86$, N=16) for aprotic solvents (Table 3 ESI, Figs 18-20 ESI) as well as for AacDMA in protic solvents ($r^2 > 0.99$, except HFiP) (Fig. 20 ESI). In both cases, an increase of solvent polarity causes decrease of the radiative rate constant. However, there is no

correlation between non-radiative rate constant and solvent polarity index (E_N^T) for all compounds studied (r^2≈0.1 or lower) (Table 3, ESI Figs 21-23 ESI). The dependence of transition dipole moment calculated according to equation[20-22]: $\mu \propto \frac{k_f}{n^2(\nu_{fluo}^{\max})^3}$ on E_N^T was also analyzed. Similar to the dependence of radiative rate constant, reasonably good correlations were obtained for all compounds studied (r^2≈0.9) in aprotic solvents as well as for AacDMA in protic ones (MeOH, EtOH, iPrOH) (Table 3 ESI, Figs 24-26 ESI). Thus, the decrease of fluorescence quantum yield and increase of fluorescence lifetimes with increase of solvent polarity are caused by the decrease of transition dipole moments.

5.2 Multiple-linear correlation

The results of multiple-linear correlation according to Catalán equation are presented in Tables 4-6 ESI. For absorption maxima of 1NacDMA good correlation was obtained (r^2≈0.95) with the largest impact of solvent polarizability (76%). For 2NacDMA and AacDMA, correlations are worse (r^2≈0.72 and r^2≈0.86, respectively). In both cases the largest impact on ν_{abs}^{max} have solvent polarizability (49% and 74%, for 2NacDMA and AacDMA, respectively) causing bathochromic shift of spectra and solvent acidity (about 20%) causing the opposite effect. Thus, the large value of a_{SP} coefficient in comparison to the others, indicates that the changes of ν_{abs}^{max} may reflect primarily change of the chromophore. Emission maximum and Stokes shift correlate well with Catalán solvent polarity scale for all compounds studied (Tables 4-6 ESI). Solvent dipolarity (60%) and polarizability (30%) play major roles in the bathochromic shift of emission spectra whereas solvent dipolarity (>60%) is the main parameter responsible for the increase of the Stokes shift. Fluorescence quantum yield correlates well with Catalan solvent polarity scale (r^2≈0.94 for 1NacDMA and

2NacDMA, $r^2 \approx 0.78$ for AacDMA) and all four solvent parameters are important from a statistical point of view. A weak correlation ($r^2 \approx 0.75$) of fluorescence lifetime for all studied compounds is obtained. However, reasonably good correlation ($r^2 \geq 0,81$) for radiative rate constant is observed. It depends mostly on solvents dipolarity (>70%) (Table 4-6). Non-radiative rate constant, contrary to the radiative one, does not depend on dipolarity of solvent. The highest impact on it has solvent acidity (83% for 1NacDMA, and 80% for 2NacDMA, $r^2 \approx 0.96$). A more complex relationship exists in the case of AacDMA for which non-radiative rate constant depends on all solvent parameters except the solvent polarizability, wherein the solvent acidity (55%) and basicity (29%) ($r^2 > 0.78$) are predominant ones. There is no correlation of transition dipole moment with Catalán solvent polarity parameters for naphthalene derivatives, while relatively good correlation for AacDMA is observed ($r^2 > 0.86$). For this compounds the transition dipole moment depends mostly on solvent dipolarity (56%, with negative sign) and solvent basicity (28%, with positive sign).

Thus, multi-linear correlation for compounds with extended π-electron system pointed out that solvent polarizability has dominant influence on position of absorption spectra, whereas the solvent dipolarity on other photophysical quantities. The exception is non-radiative rate constant which depends on solvent acidity which is associated with the formation of hydrogen bonds between solvent molecules and the free electron pair of the nitrogen atom of amino group. This conclusions are consistent with the literature data[17,20-22,28-31]. Multiple-linear correlations using Kamlet-Taft solvent polarity scale were also carried out (Tables 7-9 ESI). However, it leads to similar conclusions as obtained using Catalán solvent polarity scale. Moreover, both offer comparable quality of the fit.

5.3 Specific interactions

Hydrogen bonding as a site-specific interaction is central to understanding microscopic structures in many molecular systems, such as hydrogen-bonded water or alcohol network[48]. To extract the contribution of specific interactions between solute and hydrogen-bonding solvents the method based on solvatochromic data, proposed by Maciejewski et al.[28-31] using eq. (6), was applied. In Figs 8-10, the solvatochromic plot of position of ν_{abs}^{max} or ν_{fluo}^{max} versus Bilot-Kawski solvent polarizability function $f_{BK}(\varepsilon,n^2)$ given by eq. (9) are presented.

In these figures points corresponding to hydrocarbons, 1-chloro-n-hydrocarbons and alcohols are only shown. The best linear fit (solid line for the absorption, broken line to emission maxima) corresponds to the points representing 1-chloro-n-hydrocarbon solvents. In the cases of 1NacDMA (Fig. 8) and AacDMA (Fig.10), the points representing saturated hydrocarbons and toluene deviate from linear dependence. This deviation can be explained by the difference of interaction energy of 1-chloro-n-hydrocarbons which have permanent dipole moment and can interact with permanent and induced dipole moment of solute. The saturated hydrocarbons can interact only through dispersion interactions (except toluene which has permanent dipole moment but stacking interactions with compounds studied cannot be ruled out). For 2NacDMA, the difference in energy interactions between these two groups of solvents can be neglected, therefore, both of them were included in the calculation of hydrogen bond energy changes (Fig. 9). According to eq. (6) the distance between the straight line and experimentally determined ν_{abs}^{max}(exp) or $\nu_{\mathrm{fluo}}^{\mathrm{max}}$(exp) describes the changes in the energy of the hydrogen bond formed by solute in a given solvent. If the corresponding points are below the line, it means that this energy is greater in the excited state. In Figs 8-10, points corresponding to the position of maximum of absorption in TFE and HFiP lie above the straight line,

whereas for EtOH, iPrOH and MeOH practically coincide with a straight line in both absorption and emission. Moreover, since the position of these points coincide with other polar solvents (Figs 27-29 ESI), it can be assumed that the hydrogen bond energy does not change in the excited state (probably due to the fact that the hydrogen bonds are weak) and that they behave like polar aprotic solvents. Thus, only TFE and HFiP have appropriate proton-donor strength (see Table 1 ESI for Kamlet-Taft and Catalán solvent acidity index) to create a strong hydrogen bond with the amino group coupled to an aromatic system.

The experimentally observed position of ν_{abs}^{max} =23970 cm^{-1} for AacDMA in HFiP is higher than ν_{abs}^{max} $f_{BK}(\varepsilon,n^2)$=22975 calculated from solvatochromic plot for $f_{BK}(\varepsilon,n^2)$=0.811, that means that the energy of the hydrogen bond is 995 cm^{-1} weaker in the excited Franck-Condon state than in S_0 ground state. Similarly, for 1NacDMA and 2NacDMA hydrogen bond energy in the Franck-Condon state decreases for 1570 cm^{-1} and 3065 cm^{-1}, respectively. In the case of TFE, these values are 1120 cm^{-1}, 2285 cm^{-1} and 900 cm^{-1} for 1NacDMA, 2NacDMA and AacDMA, respectively. The weakest hydrogen bond is observed for 2NacDMA. It means that the charge transfer from amino group to aromatic naphthyl substituent in the Franck-Condon excited state is greatest among compounds studied. The solvatochromic plot of emission data of compounds studied in 1-chloro-n-alkanes (Fig 8-10) shows that the non-specific interactions in the relaxed excited state are significantly stronger and stabilize the relaxed excited state compared to the Franck-Condon state. Moreover, for naphthalene derivatives, solvent relaxation does not cause any additional changes of hydrogen bond energy even in a strong hydrogen donor as TFE. Thus, total hydrogen bond energy change occurs in the Franck-Condon excited state (Figs 27,28 ESI). More complex interactions are between TFE and AacDMA for which

emission spectra consists of two bands. For low-wavenumber emission band ν_{fluo}^{max}(exp) is below a straight line defining the non-specific interactions indicating on the increase of hydrogen bond energy ($\nu_{\mathrm{fluo}}^{\mathrm{max}}$(H-bond)=1480 cm^{-1}). However, this point is located together with other polar solvents (Fig 29 ESI), thus, it can be regarded as non-specific interactions. The structured, higher-wavenumber band practically coincides with a spectrum of AacDMA in acidified TFE (Fig. 2 ESI), and hydrogen bond energy changes calculated for it decreases for about 4560 cm^{-1}. A distinct change of hydrogen bond energy in relaxed excited state for all compounds studied is observed in HFiP (Figs 8-10). The decrease of hydrogen bond energy in this solvent is equal to 4350 cm^{-1} for 1NacDMA, 4030 cm^{-1} for 2NacDMA and 3830 cm^{-1} for AacDMA. Emission spectra of naphthalene derivatives in HFiP are red-shifted compared to that measured in acidified TFE. Moreover, they have significantly larger half-width than protonated ones and a tail at low-wavenumber side indicating on the emission of different hydrogen-bonded individuals in this solvent. Narrow and structured emission spectrum of AacDMA in HFiP indicates that this solvent forms a strong hydrogen bond with AacDMA.

In summary, the weakest hydrogen-bond in the excited state is for 2-naphthyl derivative. Its means that the charge transfer form amino group to polycyclic hydrocarbon moiety is the highest in this case. Thus, for this derivative one can expect the greatest changes in the dipole moment in the excited state. Secondly, only HFiP is able to form strong hydrogen bond with aromatic amino group in the excited state.

5.4 Excited state dipole moment

Dipole moment of molecule in the excited state is determined by the effect of electric field (internal or external) on the position of its spectral band. The method depending on the internal electric field (solvatochromism) has been frequently employed. Herein, solvent dependence of absorption and emission spectra is used to estimate the excited state dipole moment based on the Bilot-Kawski theory. Figures showing the dependence of the Stokes shift on solvent polarizability function $f_{BK}(\varepsilon,n^2)$ according to eq. (7) and sum of absorption and emission wavenumber (ν_{abs}^{max}+$\nu_{\mathrm{fluo}}^{\max}$) on ($f_{BK}(\varepsilon,n^2)+2g(n)$) according to eq. (8) are presented in ESI (Figs 30,31 ESI for 1NacDMA, Figs 32,33 ESI for 2NacDMA and Figs 34,35 ESI for AacDMA). Calculated values of the dipole moments in the excited state and the angles between the dipole moments of the ground and excited state are summarized in Table 4. Because solvent polarizability function given by eqs (9) and (10) changes mostly for electric permittivity ε ranging from 2 to 10 [33], the excited state dipole moment was calculated using data obtained for 1-chloro-n-hydrocarbon solvents for which ε changes in the range from 3.7 to 8.59 (Table 1 ESI). The change of the dipole moment in the first excited state comparing to that in the ground state is significant for all studied compounds. The biggest change is observed for 2NacDMA, $\Delta\mu$=10.2 D, then for 1NacDMA, $\Delta\mu$=7.4 D and the smallest for AacDMA $\Delta\mu$=5.6 D. Such large change of the dipole moment in the excited state and the high value of the angle between the dipoles in the ground and excited states (54º, 60º and 70º for 1NacDMA, 2NacDMA and AacDMA, respectively) indicate a substantial change in the charge distribution in the excited molecules. A larger dipole moment for 2NacDMA can be associated with a relatively large charge transfer and greater distance between charge separated in comparison to 1NacDMA. A smaller dipole moment obtained for AacDMA comparing to 1NacDMA can be explained by widespread charge

delocalization on anthracene moiety. Taking into account also non-polar solvents, lower values of dipole moment changes (about 1D) were obtained (Table 4). The change in the dipole moment is not too large, contrary to changes of angles between dipoles. Taking into consideration all solvents studied (except HFiP and 1,4-dioxane due to the fact that it behaves as a pseudo-polar solvent of variable polarizability function, which depends upon the solute`s electric field, as a result of conformation polarizability[49]) in dipole moment calculations result in large changes of both dipole moment and angle between dipoles are determined (Table 4). Because solvatochromic method uses the extrapolation technique of the linear fit to the experimental data corresponding to gaseous phase, the obtained dipole moment is for isolated, free from solvent, molecule[34]. Therefore, the dipole moments and the angles between the dipole moments in the ground and excited states received from solvatochromic effect using 1-chloro-n-alkanes seem to be correct. For polar solvents and toluene, the large deviations of ν_{fluo}^{max} from the straight line, defining the non-specific interactions are determined (Figs 27-29 ESI). Therefore, solvents exhibiting the short range specific interactions with solute molecule should be excluded. Rejection of toluene as a solvent can be justified by the additional staking type of interaction with studied compounds. Moreover, the remaining polar solvents carrying several bond dipoles appear locally more polar to studied molecules than expected on the basis of bulk electric permittivity that depends on the vector sum of group moments causing scattering of points around the fitted straight line[50].

Excited state dipole moment change can be also calculated using the relation between Stokes shift and E_N^T solvent polarity parameter according to eq. (3). Thus, obtained values presented in Table 4 are comparable (about 1D to 2D larger) to those obtained from solvatochromic shift applying all, polar and non-polar solvents.

5.5 Theoretical calculation

Using DFT and TD DFT methods, the optimized geometry, vertical transitions and transition dipole moments in absorption of compounds studied were calculated. Performed calculations reveal that all compounds studied in both, the ground and excited states, adopt a planar conformation (Figs 36-41 ESI which present the HOMO and LUMO orbitals). The energy barrier of rotation presented in Fig. 42 ESI for AacDMA indicates that the polarity of the solvent has not much influence on the energy barrier in the ground state. For permittivity ε=37.5 (acetonitrile), it is greater than (ΔE=6.55±0.14 kJ/mol) for ε=2 (cyclohexane) (ΔE=4.79±0.05 kJ/mol). These differences can be explained by the change of the bond lengths occurring in the molecule, mainly in N,N-dimethylaniline part, as well as by different solvation effect of polar dimethylamino group. In the excited state, the energy barrier of rotation increases to ΔE=7.39±0.11 kJ/mol (*in vacuo* as COSMO module is not implemented in Turbomole for the excited state calculations). Calculated vertical transitions in absorption generally reflect the shape of the absorption bands, but they are shifted bathochromically. The smallest bathochromic shift (between vertical transitions calculated for ε=2 and ε=37.5) is observed for 1NacDMA ($\Delta\lambda$=2 nm), then for 2NacDMA ($\Delta\lambda$=15 nm), and then for AacDMA ($\Delta\lambda$=16 nm) (Figs 43-45 ESI). It is worth noting that the long-wavelength transition is a pure transition between HOMO and LUMO orbitals. The transition dipole moment obtained for the long-wavelength transition is comparable for all compounds studied and equal to 7.56 D, 7.67 D and 6.93 D for 1NacDMA, 2NacDMA and AacDMA, respectively. Values of the dipole moments in the excited states calculated using DFT method (Table 4) are comparable to these obtained from solvatochromic method. Moreover, their large values result from significant charge transfer from N,N-dimethylaniline part to an

aromatic hydrocarbon part (Figs 46-48 ESI). Additionally, the redistribution of electron density due to electron excitation causes changes of the bond lengths in the molecule (Figs 49-51 ESI). The largest changes in bond lengths occur in the aromatic hydrocarbon substituents as well as within the acetylene linker. The triple bond becomes weaker, while the single bonds become stronger. This explains the increase of rotational energy barrier in the excited state. However, DFT method fails in the case of charge transfer compounds, and compounds with a large π-electron coupling[51,52]. Due to the fact that these type of compounds are studied here, the results obtained from theoretical calculations presented above should be regarded as a qualitative rather than a quantitative analysis.

6. Conclusion

Among three different solvent polarity scales used in this work, Reichardt`s empirical one is a quite useful and easy to apply, but it does not reflect the complexity of solute-solvent interactions. However, it allows for a clear distinction between protic and aprotic solvents for both absorption and emission as well as distinguish processes on which the greatest influence have electrostatic interactions. Moreover, the estimation of the excited state dipole moment change basing on the Stokes shift dependence on E_N^T is possible. Another two solvent polarity scales are more useful and allow to estimate the impact of various solvent parameters on studied quantity. Four-parameter scale has advantage over the Kamlet-Taft scale since it allows to assess independently the impact of both the polarizability and dipolarity.

The study shows that solvent polarizability has major influence on absorption solvatochromism. Position of maximum of fluorescence band as well as the photophysical properties mostly depend on solvent dipolarity, except for non-radiative

rate constant which depends on solvent acidity. Among alcohols studied, only fluorinated ones are able to form a strong hydrogen bond with amino group. However, in the excited state, because of charge transfer and decrease of the charge density on the nitrogen atom, the energy of hydrogen bond decreases and only HFiP is able to form strong hydrogen bond, whereas the remaining alcohols behave as ordinary polar solvents. Calculated, basing on solvatochromic effect, the excited state dipole moment is substantially greater than that of the ground state, which rationalized the observed large solvatochromism. A substantial charge transfer from N,N-dimethylaniline to aromatic hydrocarbon group is confirmed by theoretical calculations. Calculated theoretically optimized structures in the ground and excited states are planar for all compounds studied, while energy barrier of rotation is higher in the excited state than that in the ground state. It is worth mentioning that AacDMA, contrary to 4-(9-anthryl)-N,N-dimethylaniline (ADMA), has planar conformation in both the ground and excited states and does not emit from TICT state.

Knowledge of transition dipole moments, change of the dipole moment between the ground and excited state as well as gas phase transition energy, which can be estimated from the linear extrapolation of solvatochromic plot, allows to estimate the static hyperpolarizability β(0)[16,53,54] according to the equation:

$$\beta(0) = \frac{3(M_{ge})^2 \Delta\mu}{2(hc\tilde{\nu})^2} \quad (16)$$

where: $M_{ge}, hc\tilde{\nu}, \Delta\mu$ are the transition moment, energy gap and dipole moment change between ground and excited state, respectively. Applying the values collected in this work, the following value of β(0) are calculated: $20*10^{-30}$ cm^5esu^{-1}, $28.8*10^{-30}$ cm^5esu^{-1}, $20.4*10^{-30}$ cm^5esu^{-1} for 1NacDMA, 2NacDMA and AacDMa,

respectively. These values are not large and are comparable with the values obtained for amino-stilbene or nitro-stilbene[16] or piridyl derivatives of benzimidazole[53]. According to eq. (16), the increase of β(0) the value can be achieved by introducing electron acceptor substituent increasing Δμ. However, the increase of amount of acetylene units in the linker does not increase hyperpolarizability[15].

Acknowledgments This work was financially supported under grant UMO-2011/01/B/ST4/06094 from National Science Center (NCN) (WW, CC, MW).

The publication is financed from European Social Fund as a part of the project "Educators for the elite - integrated training program for PhD students, post-docs and professors as academic teachers at University of Gdansk" within the framework of Human Capital Operational Programme, Action IV. This publication reflects the views only of the author, and the funder cannot be held responsible for any use which may be made of the information contained therein. (IB)

References:

1 M. Kivala, F. Diederich, *Acc. Chem. Res*., 2009, **42**, 235.

2 P.F. van Hutten, J. Wideman, A. Meetsma, G. Hadziioannou, *J. Am. Chem. Soc.*, 1999, **121**, 5910.

3 T. Goodson, W. Li, A. Gharavi, L. Yu, *Adv. Matter*, 1997, **9**, 639.

4 S. Pan, Q. Fu, T. Huang, A. Zhao, B. Wang, Y. Luo, J. Yang, J. Hou, *Proc. Natl. Acad. Sci. USA*, 2009, **106**, 1559.

5 A. Facchetti, *Chem. Mater.*, 2011, **23**, 733.

6 T.Y. Chu, J. Lu, J. Ding, Y. Tao, *J. Am. Chem. Soc*., 2011, **133**, 4250.

7 B. Carlotti, R. Flamini, A. Spalletti, A. Marrocchi, F. Elisei, *ChemPhysChem*, 2012, **13**, 724.

8 R. Flamini, I. Tomasi, A. Marrocchi, B. Carlotti, A. Spalletti, *J. Photochem. Photobiol. A:Chem*., 2011, **223**, 140.

9 T.-I. Ho, A. Elangovan, H.-Y. Hsu, S.-W. Yang, *J. Phys. Chem. B*, 2005, **109**, 8626.

10 S.-W. Yang, A. Elangovan, K.-C. Hwang, T.-I. Ho, *J. Phys. Chem. B*, 2005, **109**, 16628.

11 A. Elangovan, K.-M. Kao, S.-W. Yang, Y.-L. Chen, T.-I. Ho, Y.O. Su, *J. Org. Chem*., 2005, **70**, 4460.

12 A. Elangovan, H.-H. Chiu, S.-W. Yang, T.-I. Ho, *Org. Biomol. Chem*., 2004, **2**, 3113.

13 A. Elangovan, T.-Y. Chen, C.-Y. Chen, T-I. Ho, *Chem. Commun*., 2003, 2146.

14 A. Elangovan, J.-H. Lin, S.-W. Yang, H.-Y. Hsu, T.-I. Ho, *J. Org. Chem*., 2004, **69**, 8086.

15 A.E. Stiegman, E. Graham, K.J. Perry, L.R. Khundkar, L.-T. Cheng, J.W. Perry, *J. Am. Chem. Soc*., 1991, **113**, 7658.

16 D.R. Kanis, M.A. Ratner, T. Marks, *Chem. Rev*., 1994, **94**, 195.

17 P. Suppan, N. Ghoneim, *Solvatochromism*, The Royal Society of Chemistry, U. K. 1997.

18 C. Reichardt, E. Harbusch-Görnert, *Liebigs Ann. Chem.*, 1983, 721.

19 C. Reichardt, *Chem. Rev.*, 1994, **94**, 2319.

20 K. Guzow, A. Ceszlak, M. Kozarzewska, W. Wiczk, *Photochem. Photobiol. Sci.,* 2011, **10**, 1610.

21 K. Guzow, M. Czerwińska, A. Ceszlak, M. Kozarzewska, M. Szabelski, C. Czaplewski, A. Łukaszewicz, A.A. Kubicki, W. Wiczk, *Photochem. Photobiol. Sci.,* 2013, **12**, 284.

22 A. Filarowski, M. Kluba, K. Cieślik-Boczula, A. Koll, A. Kochel, L. Pandey, W. M. De Borggrave, M. van der Auweraer, J. Catalán, N. Boens*, Photochem. Photobiol. Sci*., 2011, **9**, 996.

23 J.P. Ceron-Carrasco, D. Jacquemin, C. Laurence, A. Planchat, C. Reinchardt, K. Sraidi, *J. Phys. Org. Chem*., 2014, **27**, 512.

24 M. Ravi, A. Samanta, T.P. Radhakrishnan, *J. Phys. Chem.*, 1994, **98**, 9133.

25 S. Kumar, V.C. Rao, R.C. Rostogi, *Spectrochim. Acta A*, 2001, **57**, 41.

26 M.J. Kamlet, J.-L.M. Abbound, R.W. Taft, *Prog. Phys. Org. Chem.,* 1982, **13**, 485.

27 J. Catalán, *J. Phys. Chem. B*, 2009, **113**, 5951.

28 E. Krystkowiak, K. Dobek, A. Maciejewski, *J. Photochem. Photobiol. A:Chem.*, 2006, **184**, 250.

29 E. Krystkowiak, K. Dobek, A. Maciejewski, *Photochem. Photobiol. Sci.*, 2013, **12**, 446.

30 E. Krystkowiak, K. Dobek, G. Burdziński, A. Maciejewski, *Photochem. Photobiol. Sci.*, 2012, **11**, 1322.

31 E. Krystkowiak, A. Maciejewski, *PhysChemChemPhys.*, 2011, **13**, 11317.

32 A. Kawski, in: J.F. Rabek (Ed.), *Progress in Photochemistry and Photophysics*, Vol. 5, CRC Press, Boca Raton, USA, (1992) 1.

33 A. Kawski, *Z. Naturforsch.*, 2002, **57a**, 255.

34 A. Kawski, P. Bojarski, *Spectrochim. Acta Part B*, 2011, **82**, 527.

35 K. Sonogashira, *J. Organomet. Chem.*, 2002, **653**, 46.

36 K. Sonogashira, Y. Tohda, N. Hagihara, *Tetrahedron Lett.*, 1975, **16**, 4467.

37 A. Elangovan, Y. –H. Wang, T.-I. Ho, *Org. Lett.*, 2003, **5**,1841.

38 J.R. Lakowicz, *Principles of Fluorescence Spectroscopy*, 2nd ed., Kluwer Academic/Plenum Publishers, New York, 1999.

39 U. Subuddhi, S. Haldar, S. Sankarkrkman, A.K. Mishra, *Photochem. Photobiol. Sci*., 2006, **5**, 459.

40 P.V. James, P.K. Sudeep, C.H. Suresh, K.G. Thomas, *J. Phys. Chem. A,* 2006, **110**, 4329.

41 G. Duvanel, J. Grilj, A. Schuwey, A. Gossauer, E. Vauthey, *Photochem. Photobiol. Sci*., 2007, **6**, 956.

42 A. Beeby, K.S. Findlay, A.E. Goeta, L. Porres, S.R. Rutter, A.L. Thomson, *Photochem. Photobiol. Sci.*, 2007, **6**, 982.

43 A. Rosspeintner, G. Angulo, C. Onitsch, M. Kivala, F. Deiderich, G. Grampp, G. Gescheidt, *ChemPhysChem*., 2010, **11**, 1700.

44 S. Toyota, *Chem. Rev*., 2010, **110**, 5398.

45 M.I. Sluch, A. Godt, U.H.F. Bunz, M.A. Berg, *J. Am. Chem. Soc*., 2001, **123**, 6447.

46 L.T. Liu, D. Yaron, M.I. Sluch, M.A. Berg, *J. Phys. Chem. B*, 2006, **110**, 1844.

47 L.T. Liu, D. Yaron, M.A. Berg, *J. Phys. Chem. C*, 2007, **111**, 5770.

48 G.-J. Zhao, K.-L. Han, *Acc. Chem. Res*., 2012, **45**, 404.

49 M.B.Ledger, P. Suppan, *Spectrochim. Acta A*, 1967, **23**, 3007.

50 I. Renge, *J. Phys. Chem. A*, 2010, **114**, 6250.

51 Z.-L. Cai, K. Sendt, J. R. Reamers, *J. Chem. Phys*., 2002, **117**, 5534.

52 A. Dreuw, M. Head-Gordon, *J. Am. Chem. Soc*., 2004, **126,** 4007**.**

53 J. Abe, Y. Shirai *J. Am. Chem. Soc.,* 1996, **118**, 4705.

54 Z. Pawlowska, A. Lietard, S. Aloïse, M. Sliwa, A. Idrissi, O. Poizat, G. Buntinx, S. Delbaere, A. Perrier, F. Maurel, P. Jacques, J. Abe, *PhysChemChemPhys*., 2011, **13**, 13185.

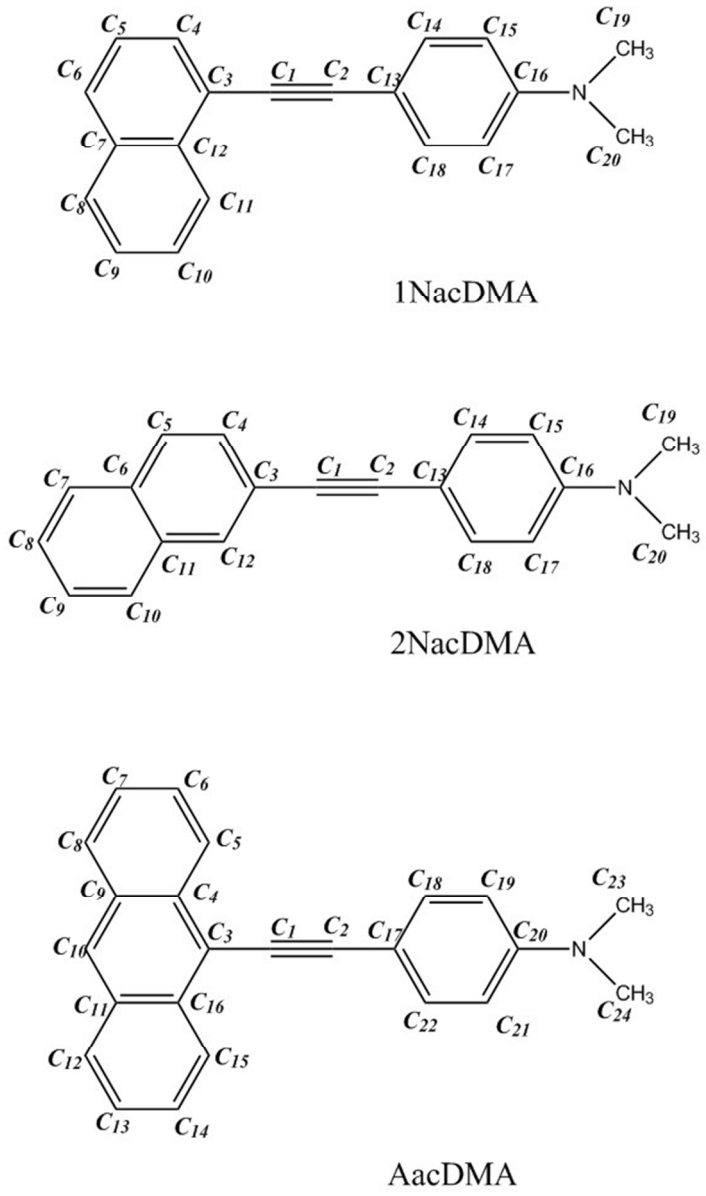

Fig. 1 Structure and atom numbering of compounds studied
120x205mm (120 x 120 DPI)

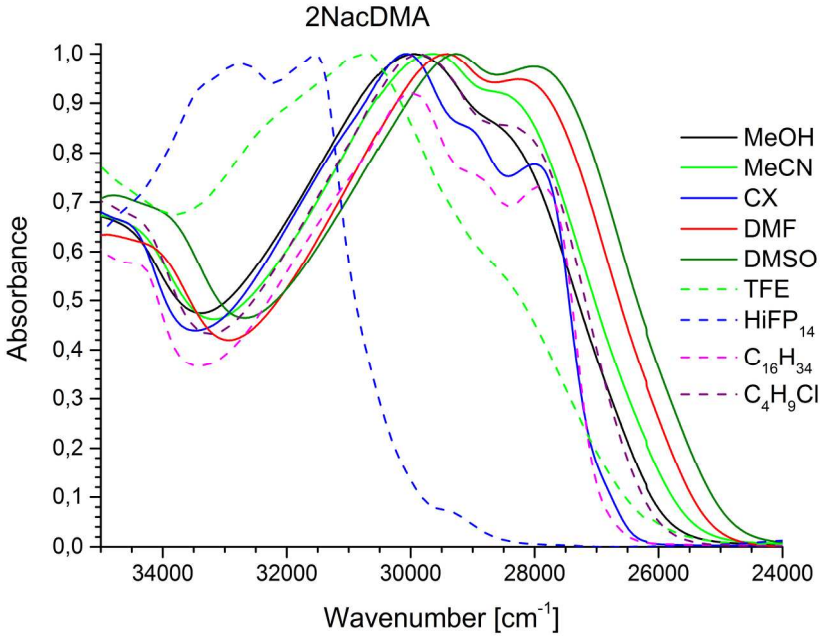

Fig. 3 Absorption spectra of 2NacDMA in selected solvents
199x139mm (300 x 300 DPI)

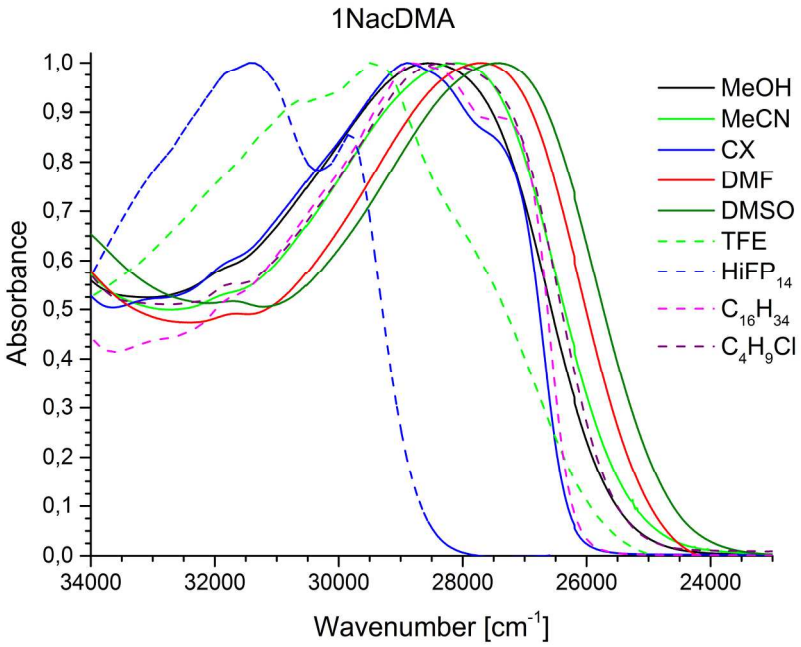

Fig. 2 Absorption spectra of 1NacDMA in selected solvents
199x139mm (300 x 300 DPI)

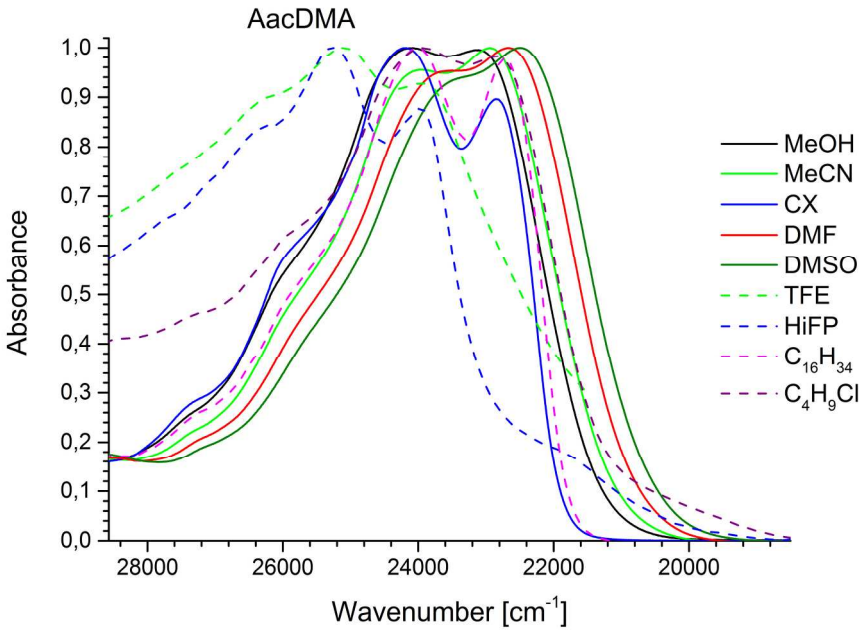

Fig. 4 Absorption spectra of AacDMA in selected solvents
199x139mm (300 x 300 DPI)

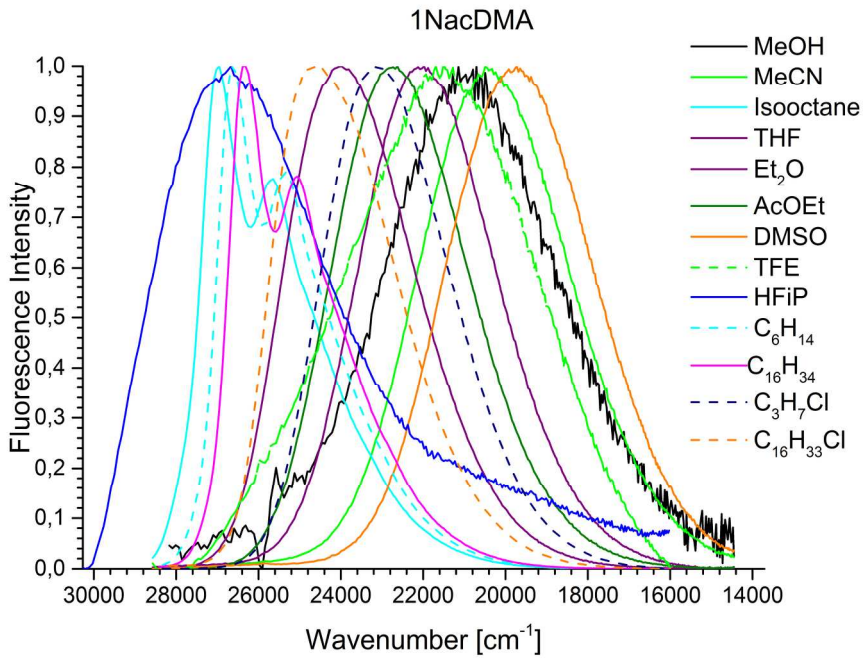

Fig. 5 Emission spectra of 1NacDMA in selected solvents
199x139mm (300 x 300 DPI)

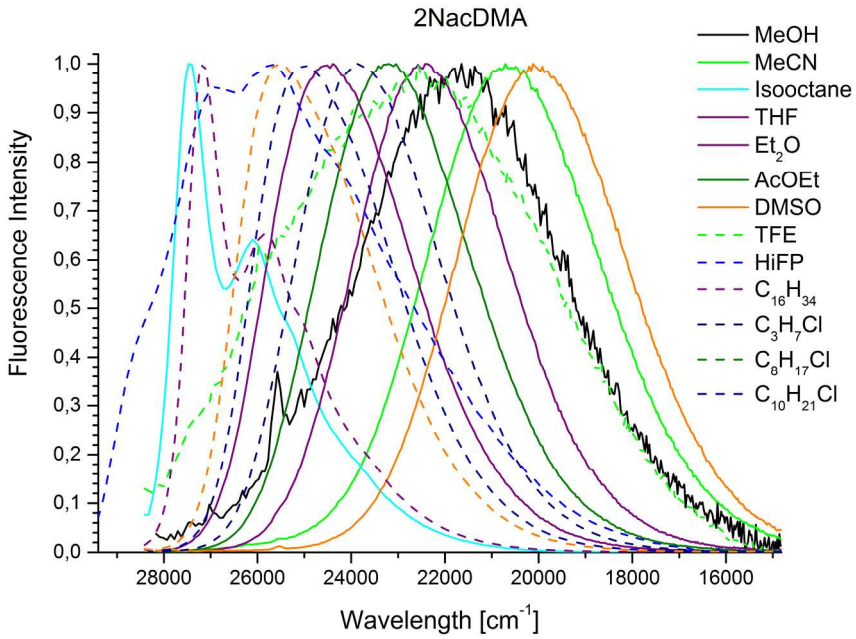

Fig. 6 Emission spectra of 2NacDMA in selected solvents
200x139mm (300 x 300 DPI)

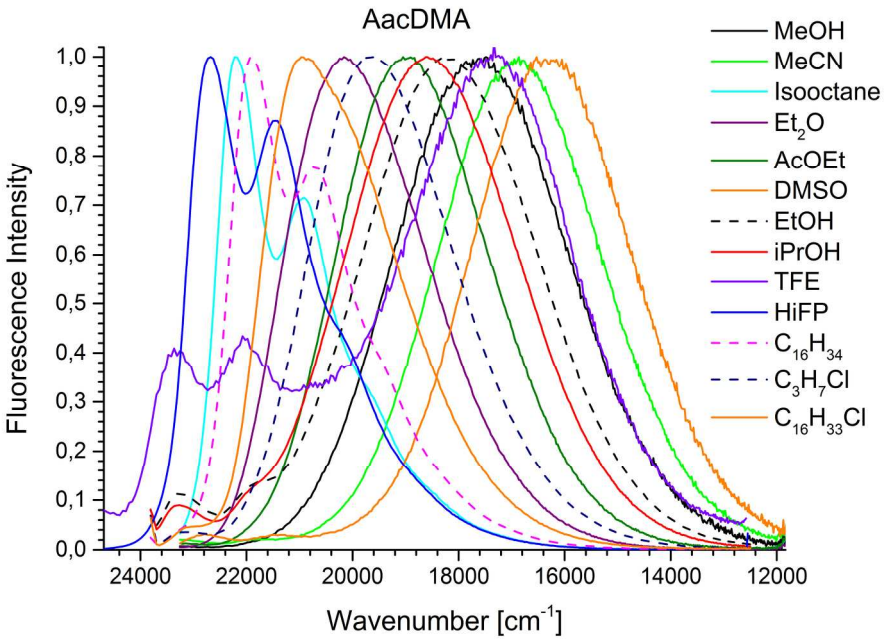

Fig. 7 Emission spectra of AacDMA in selected solvents
199x139mm (300 x 300 DPI)

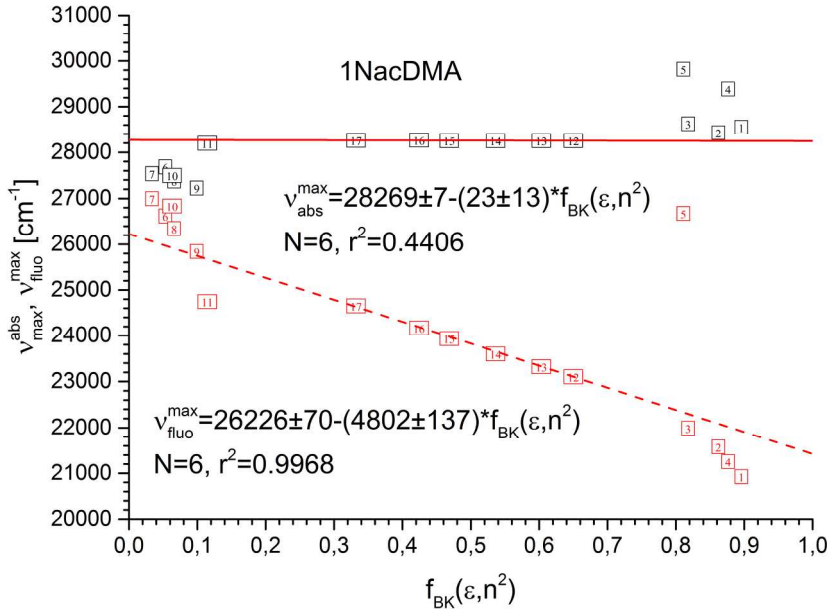

Fig. 8 The dependence of v_abs^max and v_fluo^max on the Bilot-Kawski solvent polarizability function for 1NacDMA
203x142mm (300 x 300 DPI)

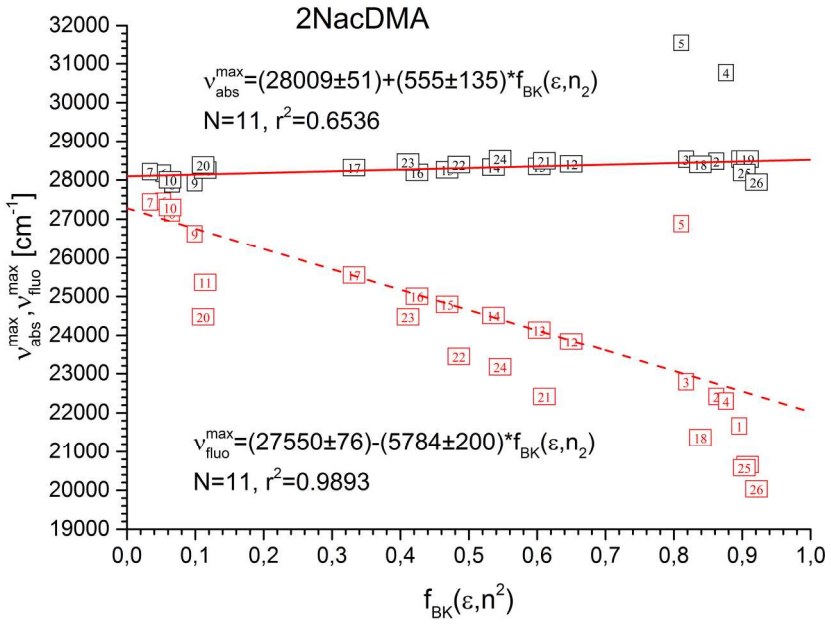

Fig. 9 The dependence of v_abs^max and v_fluo^max on the Bilot-Kawski solvent polarizability function for 2NacDMA
203x142mm (300 x 300 DPI)

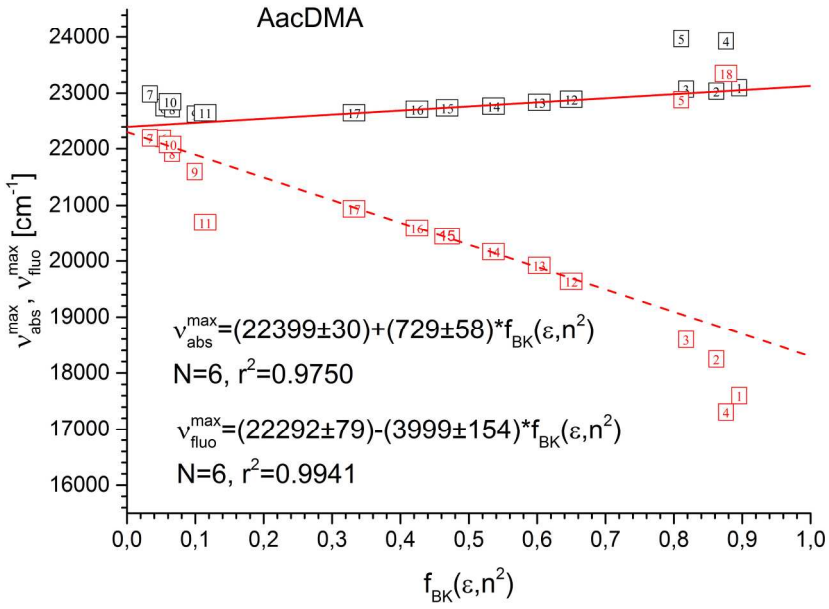

Fig. 10 The dependence of v_abs^max and v_fluo^max on the Bilot-Kawski solvent polarizability function for AacDMA.
203x142mm (300 x 300 DPI)

Table 1 The spectroscopic (maximum of absorption ν_{abs} and ν_{fluo}, and photophysical properties (Stokes shift ($\Delta\nu_{Stokes}$), fluorescence quantum yield (ϕ), fluorescence lifetime (τ), radiative (k_f), non-radiative rate constants (k_{nr})) and transition dipole moment (μ) of 1NacDMA measured in all solvents studied.

N.p.	solvent	ν_{abs} [cm^{-1}]	ν_{fluo} [cm^{-1}]	$\Delta\nu_{Stokes}$ [cm^{-1}]	ϕ	τ [ns]	k_f*10^{-8} [s^{-1}]	$k_{nr}*10^{-8}$ [s^{-1}]	$\mu*10^{5}$ [cm^3/s]
1	MeOH	28555	20927	7628	0.02	--	--	--	--
2	EtOH	28490	21577	6913	0.07	0.23	3.09	41.15	1.67
3	iPrOH	28653	21990	6663	0.11	0.37	2.97	24.05	1.46
4	TFE	29498	21250	8248	0.01	--	--	--	--
5	HFiP	31447	26673	4774	0.015	--	--	--	--
6	Hexane	29070	26618	2452	1.00	1.19	8.37	0	2.36
7	Isooctane	29070	26996	2074	0.95	1.22	7.82	0.41	2.05
8	Hexadecane	28736	26346	2390	1.00	1.39	7.18	0	1.91
9	Squalene	28490	25844	2646	1.00	1.31	7.65	0	2.10
10	Cyclohexane	28893	26835	2058	0.91	1.27	7.16	0.71	1.82
11	Toluene	28217	24746	3471	0.76	1.33	5.71	1.80	1.68
12	Chloropropane	28329	23105	5224	0.55	1.50	3.67	3.00	1.54
13	Chlorobutan	28249	23322	4927	0.94	1.42	6.61	0.42	2.65
14	Chlorohexane	28329	23600	4729	0.71	1.43	4.97	2.03	1.88
15	Chlorooctane	28249	23934	4315	1.00	1.47	6.81	0	2.43
16	Chlorodecane	28249	24168	4081	1.00	1.47	6.73	0	2.31
17	Chlorohexadecane	28249	24653	3596	1.00	1.52	6.60	0	2.09
18	Acetone	28137	21126	7011	0.44	2.57	1.71	2.18	0.98
19	Acetonitrile	28090	20404	7686	0.41	2.93	1.40	2.02	0.91
20	1.4-Dioxane	28201	23827	4374	0.70	1.53	4.58	1.96	1.67
21	THF	28098	22062	6036	0.65	1.81	3.59	1.93	1.69
22	MeTHF	28201	23032	5169	0.60	1.62	3.69	2.46	1.53
23	Et_2O	28670	24006	4664	0.63	1.44	4.37	2.57	1.73
24	AcOEt	28385	22709	5676	0.55	1.72	3.19	2.61	1.45
25	DMF	27708	20335	7373	0.57	3.40	1.68	1.27	0.97
26	DMSO	27415	19740	7675	0.62	3.91	1.54	0.94	0.92

Table 2 The spectroscopic (maximum of absorption ν_{abs} and ν_{fluo}, and photophysical properties (Stokes shift ($\Delta\nu_{Stokes}$), fluorescence quantum yield (ϕ), fluorescence lifetime (τ), radiative (k_f), non-radiative rate constants (k_{nr})) and transition dipole moment (μ) of 2NacDMA measured in all solvents studied.

N.p.	solvent	ν_{abs} [cm^{-1}]	ν_{fluo} [cm^{-1}]	$\Delta\nu_{Stokes}$ [cm^{-1}]	ϕ	τ [ns]	k_f*10^{-8} [s^{-1}]	$k_{nr}*10^{-8}$ [s^{-1}]	$\mu*10^{5}$ [cm^3/s]
1	MeOH	28528	21665	6863	0.02	--	--	--	--
2	EtOH	28476	22418	6058	0.03	1.57	1.91	61.8	0.92
3	iPrOH	28524	22794	5730	0.15	2.53	5.93	33.6	2.62
4	TFE	30769	22300	8470	0.006	--	--	--	--
5	HFiP	31546	26882	4664	0.02	--	--	--	--
6	Hexane	28169	27457	712	0.79	1.07	7.42	1.97	1.90
7	Isooctane	28211	27439	772	0.82	1.08	7.57	1.66	1.89
8	Hexadecane	27900	27158	742	1.00	1.19	8.41	0	2.04
9	Squalene	27930	26624	1306	1.00	1.04	9.62	0	2.41
10	Cyclohexane	27999	27293	706	0.88	1.14	7.74	1.06	1.87
11	Toluene	28250	25361	2889	0.98	1.12	8.78	0.18	2.40
12	Chloropropane	28409	23831	4578	0.75	1.33	5.65	1.88	2.16
13	Chlorobutane	28343	24131	4212	0.85	1.27	6.70	1.18	2.43
14	Chlorohexane	28325	24508	3817	1.00	1.27	7.88	0	2.66
15	Chlorooctane	28256	24798	3458	1.00	1.28	7.79	0	2.50
16	Chlorodecane	28187	25005	3182	1.00	1.30	7.72	0	2.39
17	Chlorohexadecane	28315	25551	2764	1.00	1.29	7.74	0	2.21
18	Acetone	28398	21366	7032	0.48	2.34	2.05	2.22	1.14
19	Acetonitrile	28528	20660	7868	0.47	2.88	1.63	1.84	1.02
20	1.4-Dioxane	28379	24475	3904	0.72	1.32	5.48	2.13	1.85
21	THF	28482	22418	6064	0.65	1.50	4.33	2.33	1.94
22	MeTHF	28390	23438	4952	0.61	1.40	4.36	2.79	1.71
23	Et_2O	28454	24475	3979	0.75	1.25	6.01	2.00	2.24
24	AcOEt	28539	23172	5367	0.55	1.46	3.76	3.08	1.60
25	DMF	28184	20583	7601	0.69	3.20	2.15	0.97	1.21
26	DMSO	27942	20034	7908	0.75	3.91	1.92	0.64	1.09

Table 3 The spectroscopic (maximum of absorption ν_{abs} and ν_{fluo}, and photophysical properties (Stokes shift ($\Delta\nu_{Stokes}$), fluorescence quantum yield (ϕ), fluorescence lifetime (τ), radiative (k_f), non-radiative rate constants (k_{nr})) and transition dipole moment (μ) of AacDMA measured in all solvents studied.

N.p.	solvent	ν_{abs} [cm^{-1}]	ν_{fluo} [cm^{-1}]	$\Delta\nu_{Stokes}$ [cm^{-1}]	ϕ	τ [ns]	k_f*10^{-8} [s^{-1}]	$k_{nr}*10^{-8}$ [s^{-1}]	$\mu*10^{6}$ [cm^3/s]
1	MeOH	23094	17600	5494	0.19	2.03	0.937	3.98	4.29
2	EtOH	23034	18246	4788	0.37	3.01	1.23	2.09	5.44
3	iPrOH	23072	18593	4479	0.60	3.98	1.51	1.01	6.44
4	TFE	23928	23422	506	0.01	*	-	-	-
5	HFiP	23969	22884	1085	0.15	**	-	-	-
6	Hexane	22738	22177	561	0.60	2.55	2.35	1.57	10.6
7	Iso-octane	22984	22189	795	0.58	2.61	2.22	1.61	9.46
8	Hexadecane	22722	21918	804	0.76	3.24	2.34	0.74	9.71
9	Squalene	22628	21596	1032	0.81	3.48	2.33	0.55	9.52
10	Cyclohexane	22847	22074	773	0.58	3.02	1.92	1.39	7.92
11	Toluene	22650	20694	1956	0.73	3.13	2.33	0.86	8.95
12	Chloropropane	22892	19637	3255	0.71	3.72	1.91	0.78	8.26
13	Chlorobutane	22835	19921	2914	0.65	3.44	1.89	1.02	8.11
14	Chlorohexane	22769	20165	2604	0.81	3.47	2.33	0.55	9.81
15	Chlorooctane	22736	20448	2288	0.68	3.61	1.89	0.89	7.84
16	Chlorodecane	22712	20591	2121	0.73	3.69	1.99	0.73	8.17
17	Chlorohexadecane	22651	20938	1713	0.71	3.72	1.91	0.78	7.82
18	Acetone	22915	17484	5431	0.39	4.50	0.87	1.36	3.90
19	Acetonitrile	22936	16891	6045	0.31	3.99	0.78	1.73	3.56
20	1.4-Dioxane	22730	20088	2642	0.82	3.97	2.06	0.45	8.69
21	THF	22778	18295	4483	0.88	4.74	1.86	0.25	7.93
22	MeTHF	22845	19147	3698	0.70	3.88	1.80	0.77	7.65
23	Et_2O	23025	20152	2873	0.76	3.52	2.16	0.68	9.67
24	AcOEt	22939	18967	3972	0.65	3.92	1.66	0.89	7.30
25	DMF	22665	16736	5929	0.38	3.99	0.95	1.56	4.00
26	DMSO	22469	16272	6197	0.34	3.75	0.91	1.76	3.66

* for λ_{obs}=455 nm τ_1=4.99, α_1=0.3117; τ_2=2.72, α_2=0.2274; τ_3=0.09, α_3=0.4609

** for λ_{obs}=455 nm τ_1=2.58, A_1=14439; τ_1=0.50, A_1=-4263 and

for λ_{obs}=590 nm τ_1=4.89, α_1=0.0461; τ_2=0.65, α_2=0.3647; τ_3=0.13, α_3=0.5882

Table 4 Values of slops (m_1 and m_2)obtained from a linear fits to equations (7) and (8), coefficient of quality of fit (r^2), dipole moment change in exited state (Δμ), and angle between dipole moments in the ground and excited state (Ψ) obtained from solvatochromic studies for 1NacDMA, 2NacDMA and AacDMA. The theoretically calculated dipole moment (μ) for ground and excited state as well as the value of Onsager a radius and change of dipole moment in excited state calculated based on eq. (3) are also presented.

1NacDMA $\mu_{calculated}$=3.73 [D], a=5.6 [A]				
N=24	m_2=8029±416; r^2=0.9442	Δμ=8.68 [D]	m_1=6099±284; r^2=0.9546	Ψ=48.37°
N=11	m_2=7391±313; r^2=0.9823	Δμ=8.42 [D]	m_1=4934±166; r^2=0.9888	Ψ=37.12°
N=6	m_2=6270±192; r^2=0.9953	Δμ=7.37 [D]	m_1=5060±196; r^2=0.9925	Ψ=53.79°
N=16	E_T^N; B=12624; r^2=0.9748	Δμ=9.04 [D]		
μ theoretically calculated in S_1 state		13.6 [D]		
2NacDMA $\mu_{calculated}$ =3.62 [D], a=6.49 [A]				
N=24	m_2=8648±556; r^2=0.8733	Δμ=12.12 [D]	m_1=7520±478; r^2=0.9188	Ψ=60.09°
N=11	m_2=5275±183; r^2=0.9893	Δμ=8.88 [D]	m_1=6344±169; r^2=0.9936	Ψ=91.77°
N=6	m_2=6541±423; r^2=0.9835	Δμ=10.19 [D]	m_1=5676±223; r^2=0.9938	Ψ=60.19°
N=16	E_T^N; B=16512; r^2=0.9378	Δμ=11.13 [D]		
μ theoretically calculated in S_1 state		17.5 [D]		
AacDMA $\mu_{calculated}$ =4.01 [D], a=5.6 [A]				
N=24	m_2=5776±415; r^2=0.8979	Δμ=6.8 [D]	m_1=5833±401; R_2=0.9056	Ψ=68.93°
N=11	m_2=3931±165; r^2=0.9837	Δμ=5.19 [D]	m_1=3952±149; R_2=0.9873	Ψ=64.47°
N=6	m_2=4400±236; r^2=0.9884	Δμ=5.62 [D]	m_1=4727±203; R_2=0.9927	Ψ=69.96°
N=16	E_T^N; B=12588; r^2=0.9530	Δμ=9.02 [D]		
μ theoretically calculated in S_1 state		9.4 [D]		